Chinese Journal of
POLYMER SCIENCE

RESEARCH ARTICLE

https://doi.org/10.1007/s10118-021-2646-4
Chinese J. Polym. Sci. **2022**, *40*, 220–230

Software Package: An Advanced Theoretical Tool for Inhomogeneous Fluids (*Atif*)

Jian Jiang[a,b*]

[a] *Beijing National Laboratory for Molecular Sciences, State Key Laboratory of Polymer Physics and Chemistry, Institute of Chemistry, Chinese Academy of Sciences, Beijing 100190, China*
[b] *University of Chinese Academy of Sciences, Beijing 100049, China*

Electronic Supplementary Information

Abstract In spite of the impending flattening of Moore's law, the complexity and size of the systems we are interested in keep on increasing. This challenges the computer simulation tools due to the expensive computational cost. Fortunately, advanced theoretical methods can be considered as alternatives to accurately and efficiently capture the structural and thermodynamic properties of complex inhomogeneous fluids. In the last decades, classical density functional theory (cDFT) has proven to be a sophisticated, robust, and efficient approach for studying complex inhomogeneous fluids. In this work, we present a pedagogical introduction to a broadly accessible open-source density functional theory software package named "an advanced theoretical tool for inhomogeneous fluids" (*Atif*) and of the underlying theory. To demonstrate *Atif*, we take three cases as examples using a typical laptop computer: (i) electric double-layer of asymmetric electrolytes; (ii) adsorptions of sequence-defined semiflexible polyelectrolytes on an oppositely charged surface; and (iii) interactions between surfaces mediated by polyelectrolytes. We believe that this pedagogical introduction will lower the barrier to entry to the use of *Atif* by experimental as well as theoretical groups. A companion website, which provides all of the relevant sources including codes and examples, is attached.

Keywords Polyelectrolytes; Complex fluids; Software; Density functional theory; Self-defined sequence

Citation: Jiang, J. Software package: an advanced theoretical tool for inhomogeneous fluids (*Atif*). *Chinese J. Polym. Sci.* **2022**, *40*, 220–230.

INTRODUCTION

Classical density functional theory (cDFT) has proven to be a versatile, powerful, efficient, and widely used method in the study of complex inhomogeneous fluids such as liquid-vapor interfaces, wetting and drying on substrates, and soft matters (including electrolytes, polymers, sequence-defined polyelectrolytes and so on) in confined geometries.[1–3] cDFT connects the microscopic structural features to the physiochemical properties of macro- and mesoscopic confined systems at a very low computational cost *via* an analytical expression for the free energy (grand potential or Helmholtz free energy) functional based on a given equation of state. In cDFT, the many-body problem is described by the unique free energy functional of the spatially varying particle for a given external potential.[4,5] Thus the complex many-body problem is reduced into a simple single-field theoretical problem. This makes cDFT calculations be generally much less expensive than particle-based simulation methods. Therefore, cDFT has a particular advantage over particle-based computer simulation methods in studies of complex inhomogeneous fluids (especially for the confined systems with multi-chain polyelectrolytes).

Dramatic progress in cDFT took place throughout the late 1970s to the early 1990s. In these two decades, the general formalism of cDFT was established for both uncharged and charged systems based on the hard-sphere model (*i.e.*, the basic units of the molecules are modeled as hard spheres or charged hard spheres) where the solvent is represented by a continuous dielectric medium (*i.e.*, the primitive model for electrolytes).[6–10] Later on, cDFT has been extended to describe uncharged[11,12] and charged[13] polymeric fluids using Wertheim's thermodynamic perturbation theory (TPT)[14–20] and its extensions.[21,22] The central task in cDFT is to construct the analytical free energy functional with respect to the density distributions of the components. Generally, the total Helmholtz free energy can be written as

$$\mathcal{F} = \mathcal{F}_{\mathrm{id}} + \mathcal{F}_{\mathrm{ex}} \quad (1)$$

where $\mathcal{F}_{\mathrm{id}}$ is the ideal part and the excess part $\mathcal{F}_{\mathrm{ex}}$ is

$$\mathcal{F}_{\mathrm{ex}} = \mathcal{F}_{\mathrm{hs}} + \mathcal{F}_{\mathrm{vdW}} + \mathcal{F}_{\mathrm{C}} \quad (2)$$

On the right-hand side of Eq. (2), the terms, from left to right, account for the hard-core excluded volume interactions, van der Waals interactions and Coulomb interactions, respectively. In general, $\mathcal{F}_{\mathrm{hs}} = \mathcal{F}_{\mathrm{hs}}^{\mathrm{o}} + \mathcal{F}_{\mathrm{hs}}^{\mathrm{ch}}$. $\mathcal{F}_{\mathrm{hs}}^{\mathrm{o}}$ is the excluded volume effects from the hard-core interactions which can be

* Corresponding author, E-mail: jiangj@iccas.ac.cn
Invited Research Article
Received August 5, 2021; Accepted September 1, 2021; Published online November 9, 2021

accurately described by fundamental measure theory (FMT)[8] and its extensions (MFMT).[23,24] The agreements between the MFMT and Monte Carlo simulations are excellent for inhomogeneous hard-sphere fluids including both one component and mixture systems for the entire range of densities.[23,24] $\mathcal{F}_{hs}^{ch}$ is the non-bonded chain connectivity correlations in the polymeric fluid systems due to hard-core interactions which can be approximated using TPT.[25] The free energy due to Coulomb interactions is

$$\mathcal{F}_C = \mathcal{F}_{MF}^C + \mathcal{F}_{el} \tag{3}$$

where $\mathcal{F}_{MF}$ is the Coulomb interactions at mean field level and $\mathcal{F}_{el}$ is the contributions from electrostatic correlations (which is beyond the mean field level). Generally, $\mathcal{F}_{el} = \mathcal{F}_{el}^{o} + \mathcal{F}_{el}^{ch}$, where $\mathcal{F}_{el}^{o}$ is the electrostatic correlations of charged hard spheres which can be approximated using the mean spherical approximation (MSA)[26–28] or a "soft correlation hole" method;[29,30] and $\mathcal{F}_{el}^{ch}$ is the the non-bonded chain connectivity due to the electrostatic correlations in the polymeric fluid systems, which can be captured using a sticky-point model.[21,22] After the construction of analytic expression of $\mathcal{F}$ in Eq. (1) is completed, one can obtain the structural and thermodynamic properties of the inhomogeneous systems by finding the extrema of the Helmholtz free energy or the grand potential (which can be obtained from the Helmholtz free energy functional *via* the Legendre transform). The details of $\mathcal{F}$ and the implementation of cDFT will be presented in the next two sections.

Although the accuracy and efficiency of cDFT in studying non-uniform complex fluids have been proven, cDFT has been neither widely used by experimental groups nor by theoretical and computational groups. The major roadblocks to the widespread use of cDFT by both experimental and theoretical/computational groups are the complexity of the theory itself and the lack of an easy-to-use software about cDFT. On the one hand, there were many different versions of cDFTs in the literature which make the researchers confused about how to make a right choice. Moreover, the learning barrier of cDFTs (such as FMT, MSA, TPT and so on) is relatively high, especially for experimental groups. On the other hand, the absence of an easy-to-use and robust software makes the implementation of cDFT be difficult to our chemical physics and physical chemistry communities. Although the Sandia National Laboratories in USA has released a software named "Tramonto" based on cDFT in 2000s,[31] the cumbersome software package and complicated installation process make the entry barrier of "Tramonto" extremely high. Furthermore, the last version of "Tramonto" was released in 2011. In the past decade, impactive progress has been made in both cDFT itself and its applications which were not involved in "Tramonto". Therefore, an easy-to-use and broadly accessible software based on the up-to-date cDFT is requisite.

cDFT has experienced half a century of development. The pedagogy for cDFT framework is now reasonably mature. In this work, we provide a pedagogical introduction to the open-source software named "an advanced theoretical tool for inhomogeneous fluids" (*Atif*) developed by us, and the details of the underlying theory are also introduced. Here "advanced" means more accuracy and efficiency. The comparisons between *Atif* and other methods are shown in Sec. IV. Using *Atif*, one can study the structural, thermodynamic, and electrochemical properties (such as electric double-layer, capacitance, adsorption behaviors, interactions between two surfaces and so on) of inhomogeneous complex fluids (including uncharged hard-sphere fluids, electrolytes with symmetrical/asymmetrical size and multivalency, charged/uncharged flexible/semiflexible block/sequence-defined polymers and polymer blends and so on) in the vicinity of a single surface or confined by two surfaces. Moreover, *Atif* integrates both cDFT and a self-consistent field theory (SCFT).[32,33] The users can choose one of the two methods arbitrarily to start their projects. In order to make it unnecessary for users to either know the computer language (such as C++ or FORTRAN) or seek an experienced collaborator, this designed software can be controlled completely *via* a readable input file. Even people who know nothing about computer language can install successfully and run their first example on their laptop in minutes. *Atif* is compiled using C++ and it is very easy to be extended. If one is interested in the theory itself and wants to contribute to *Atif*, one can integrate his/her own subroutines into *Atif* easily.

To demonstrate *Atif* clearly, we take three cases as examples. In the first example, we study the electric double-layer of electrolytes with asymmetrical size in the vicinity of a charged surface. In the second one, we present the adsorption behaviors of semiflexible sequence-defined polyelectrolytes on an oppositely charged surface. In the third one, we show the interactions between two charged surfaces mediated by polyelectrolytes.

This study is organized as follows. In the next section we introduce the formalism and model considered in *Atif*. In Sec. III, the installation and implementations of *Atif* are described. In Sec. IV, we consider the three examples one by one to further demonstrate the implementations of *Atif*. Sec. V contains our conclusions and outlook.

MODEL AND THEORY

In general, the system in *Atif* can contain charged/uncharged flexible/semiflexible homopolymers, copolymers, sequence-defined polymers, charged/uncharged small molecules. To simplify the demonstration, we present the cDFT equations in this work for the case of charged semiflexible sequence-defined polymer blends with salts in the vicinity of a charged surface. Assume that the system contains P species of sequence-defined polymers, where each polymer has N_p blocks and the m^{th} block of the p^{th} polymer consists of N_p^m monomers with $p \in [1, \cdots, P]$ which is the index of different species of polymers and $m \in [1, \cdots, N_p]$ which is the index of different blocks. We start our discussions by considering the grand potential of the system. The grand potential can be obtained from the Helmholtz free energy functional *via* the Legendre transform, *i.e.*,

$$W = \mathcal{F}_{id} + \mathcal{F}_{ex} + \sum_{p=1}^{P} \int d\mathbf{R} \rho_p(\mathbf{R}) \left[\psi_p(\mathbf{R}) - \mu_p \right] + \sum_{\alpha} \int d\mathbf{r} \rho_\alpha(\mathbf{r}) \left[\psi_\alpha(\mathbf{r}) - \mu_\alpha \right] \tag{4}$$

where $d\mathbf{R} = d\mathbf{r}_1 d\mathbf{r}_2 \cdots d\mathbf{r}_{\mathcal{N}_p}$, and $\rho_p(\mathbf{R})$ is the $3\mathcal{N}_p$-dimensional density distribution of the polymer p with $\mathcal{N}_p = \sum_{m=1}^{N_p} N_p^m$ as the polymerization. In this work, the subscript α refers to

small ions only and p refers to entire polymers, and hereinafter the subscript i or j refers to small ions (including salts and counterions) and monomers. μ_p and μ_α are the chemical potentials of the entire polymers and small ions, respectively. The non-electrostatic external potential $\Psi_p(\mathbf{R})$ is applied to the entire chain of the p^{th} polymers, *i.e.*, $\Psi_p(\mathbf{R}) = \sum_{m=1}^{N_p}\sum_{k=1}^{N_p^m}\psi_{p,m}(\mathbf{r}_{p,m}^k)$, where k is the index of monomer and $\psi_{p,m}$ is the external potential imposed on the individual segments. $\psi_\alpha(\mathbf{r})$ is the non-electrostatic external potential for small ions. The non-electrostatic external potential in *Atif* is modeled as Square-well (SW) or 9-3 Lennard-Jones potential as shown in Sec. I in the electronic supplementary information (ESI).

In this work, the semiflexible sequence-defined polymers are modeled as $\mathcal{N}_p$ tangentially connected hard spheres (monomers) with diameter and valency of the monomers in the m^{th} block of the p^{th} polymer being σ_p^m and z_p^m, respectively. We assume that the salts and counterions are modeled as charged hard spheres with diameter σ_α and valency z_α; and the solvent is treated as a continuum dielectric background with dielectric constant ε_r. We have to note that the set $\{\sigma_i\}$ or $\{\sigma_j\}$ is equal to $\{\sigma_p^m\}\bigcup\{\sigma_\alpha\}$ and $\{z_i\}$ or $\{z_j\}$ is equal to $\{z_p^m\}\bigcup\{z_\alpha\}$. The schematic of the model under consideration in this work is shown in Fig. 1.

In Eq. (4), the ideal free energy is given by

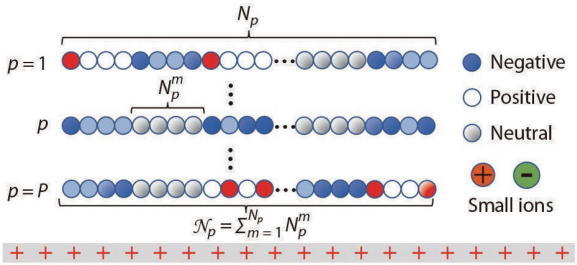

Fig. 1 Schematic of the model under consideration in this work. The connected spheres are the semiflexible sequence-defined polymers, where the red, blue, and light gray beads are the positively charged, negatively charged, and neutral monomers, respectively. The isolated dark orange (positive) and green (negative) spheres denote the counterions and salts; and the gray filling rectangle is the structureless, charged, planar, and impenetrable surface.

$$\begin{aligned}\beta\mathcal{F}_{\text{id}} =& \sum_{p=1}^{P}\int \mathrm{d}\mathbf{R}\rho_p(\mathbf{R})\left\{\ln\left[\rho_p(\mathbf{R})\Lambda_p\right]-1\right\}+\\ &\sum_{p=1}^{P}\int \mathrm{d}\mathbf{R}\rho_p(\mathbf{R})\beta\left[V_p^{\text{b}}(\mathbf{R})+U_p^{\text{b}}(\mathbf{R})\right]+\\ &\sum_{\alpha}\int \mathrm{d}\mathbf{r}\rho_\alpha(\mathbf{r})\left\{\ln\left[\rho_\alpha(\mathbf{r})a_\alpha\right]-1\right\}\end{aligned} \tag{5}$$

with $\Lambda_p = \pi_{m=1}^{N_p}(a_p^m)^{N_p^m}$, where a_p^m and a_α are volume scale which can be taken as the cube of the thermal de Broglie length; the precise definition of a_p^m and a_α are immaterial as they have no thermodynamic consequences. Therefore, for simplicity, we set $a = a_p^m = a_\alpha$. In order to explain the bonding and bending potentials clearly, we redefine the monomer index k: $1 \le k \le \mathcal{N}_p$ for polymer p. Then the bonding potential $V_p^{\text{b}}(\mathbf{R})$ in the ideal part (Eq. (5)) is written in the form

$$\exp\left[-\beta V_p^{\text{b}}(\mathbf{R})\right] = a^{\mathcal{N}_p-1}\prod_{k=1}^{\mathcal{N}_p-1}\frac{\delta(|\mathbf{r}_p^k-\mathbf{r}_p^{k+1}|-d_p^k)}{4\pi(d_p^k)^2} \tag{6}$$

where $\mathbf{r}_p^k$ is the spatial coordinate of the k^{th} monomer of the p^{th} polymer. The bending potential $U_p^{\text{b}}(\mathbf{R})$ in the ideal part (Eq. 5) is commonly approximated using the Kratky-Porod (KP) wormlike chain (WLC) model.[34–39] The Hamiltonian of KP WLC (hereafter referred to as WLC) is $\beta\mathcal{H} = \frac{\kappa_{\text{b}}}{2}\int_0^L \mathrm{d}s(\mathrm{d}^2\mathbf{r}(s)/\mathrm{d}^2 s)^2$ with $\mathbf{r}(s)$ the chain in continuum space and $\beta = 1/(k_{\text{B}}T)$ is the inverse thermal energy with k_{B} the Boltzmann constant. The local rigidity of the polymer chain is determined by a single parameter---the bending modulus κ_{b} with $l_{\text{p}} \propto \kappa_{\text{b}}$, where l_{p} is the persistence length of the polymer. In this work, we make use of the discrete version of WLC. The bending potential is

$$\exp\left[-\beta U_p^{\text{b}}(\mathbf{R})\right] = \prod_{k=1}^{\mathcal{N}_p-2}\exp\left[-\beta E_{\text{b}}(\mathbf{s}_p^k,\mathbf{s}_p^{k+1})\right] \tag{7}$$

where $E_{\text{b}}(\mathbf{s}_p^k,\mathbf{s}_p^{k+1})$ is the bending potential between two successive bonds, *i.e.*,

$$\beta E_{\text{b}}(\mathbf{s}_p^k,\mathbf{s}_p^{k+1}) = \kappa_{\text{b}}\left(1-\frac{\mathbf{s}_p^k\cdot\mathbf{s}_p^{k+1}}{d_p^k d_p^{k+1}}\right) \tag{8}$$

where $\mathbf{s}_p^k = \mathbf{r}_p^{k+1} - \mathbf{r}_p^k$ is the bond vector between two successive monomers. In Eqs. (6) and (8), d_p^k is the bond length, where $d_p^k = \sigma_p^m$ for $\sum_{\hat{m}=1}^{m-1}N_p^{\hat{m}} < k < \sum_{\hat{m}=1}^{m}N_p^{\hat{m}}$ with $\sum_{\hat{m}=1}^{0}N_p^{\hat{m}} = 0$ and $d_p^k = (\sigma_p^m + \sigma_p^{m+1})/2$ for $k = \sum_{\hat{m}=1}^{m}N_p^{\hat{m}}$. This discrete WCL model has been widely used for simulations and theoretical studies of semiflexible chains,[40–48] and its success has already been proved by the molecular dynamics[40] and Monte Carlo (MC) simulations.[41,43]

As discussed in the section above, the excess free energy density can be written as

$$\mathcal{F}_{\text{ex}} = \mathcal{F}_{\text{hs}}^{\text{o}} + \mathcal{F}_{\text{el}}^{\text{o}} + \mathcal{F}_{\text{hs}}^{\text{ch}} + \mathcal{F}_{\text{el}}^{\text{ch}} + \mathcal{F}_{\text{MF}}^{\text{C}} + \mathcal{F}_{\text{vdW}} \tag{9}$$

The excess free energy due to the hard-core excluded volume effect, $\mathcal{F}_{\text{hs}}^{\text{o}}$, is calculated using MFMT,[8,23,24] which is given by

$$\mathcal{F}_{\text{hs}}^{\text{o}}[\{\rho_\alpha(\mathbf{r})\}] = \int \mathrm{d}\mathbf{r}\Phi_{\text{hs}}^{\text{o}}[\{n_l(\mathbf{r})\}] \tag{10}$$

where

$$\begin{aligned}\beta\Phi_{\text{hs}}^{\text{o}}[\{n_l(\mathbf{r})\}] =& -n_0\ln(1-n_3)+\frac{n_1n_2-\vec{n}_1\cdot\vec{n}_2}{(1-n_3)}+\\ &\frac{n_2^3-3n_2\vec{n}_2\cdot\vec{n}_2}{36\pi}\left[\frac{\ln(1-n_3)}{n_3^2}+\frac{1}{n_3(1-n_3)^2}\right]\end{aligned} \tag{11}$$

The weighted densities $\{n_l(\mathbf{r})\}$ are

$$n_l(\mathbf{r}) = \sum_i\int \rho_i(\mathbf{r}')w_l(\mathbf{r}-\mathbf{r}';R_i)\mathrm{d}\mathbf{r} \tag{12}$$

where the radius R_i is $R_i = \sigma_i/2$. We have $\{\rho_i(\mathbf{r})\} = \{\rho_p^m(\mathbf{r})\}\bigcup\{\rho_\alpha(\mathbf{r})\}$, where the density distribution of the monomers in the m^{th} block of the p^{th} polymer is

$$\rho_p^m(\mathbf{r}) = \sum_{k=1}^{N_p^m}\int \mathrm{d}\mathbf{R}\delta(\mathbf{r}-\mathbf{r}_{p,m}^k)\rho_p(\mathbf{R}) \tag{13}$$

In Eq. (12), the weighted functions $w_l(\mathbf{r};x)$ are

$$w_3(\mathbf{r};x)=\Theta(x-|\mathbf{r}|),\ w_2(\mathbf{r};x)=\delta(x-|\mathbf{r}|)$$
$$\vec{w}_2(\mathbf{r};x)=\frac{\mathbf{r}}{|\mathbf{r}|}\delta(x-|\mathbf{r}|),\ \vec{w}_1(\mathbf{r};x)=\frac{\vec{w}_2(\mathbf{r};x)}{4x} \quad (14)$$
$$w_1(\mathbf{r};x)=\frac{w_2(\mathbf{r};x)}{4x},\ w_0(\mathbf{r};x)=\frac{w_2(\mathbf{r};x)}{4x^2}$$

where $\Theta(\mathbf{r})$ and $\delta(\mathbf{r})$ is the Heaviside function and Dirac's delta function, respectively.

As presented in our previous work,[49] we construct the free energy due to the electrostatic correlations $\mathcal{F}_{\mathrm{el}}^{\mathrm{o}}$ using four FMT-like weighted densities $\{q_i^{(l)}\}$, *i.e.*,

$$q_i^{(l)}(\mathbf{r})=\left(\frac{R_i}{\lambda_i}\right)^l\int\rho_i(\mathbf{r}')w_l(\mathbf{r}-\mathbf{r}';\lambda_i)\mathrm{d}\mathbf{r} \quad (15)$$

where $\lambda_i=R_i+1/2\Gamma_{\mathrm{b}}$ with Γ_{b} the screening length parameter for the bulk systems in MSA. Then the functional for electrostatic correlations is given by

$$\mathcal{F}_{\mathrm{el}}^{\mathrm{o}}[\{\rho_i(\mathbf{r})\}]=\int\mathrm{d}\mathbf{r}\Phi_{\mathrm{el}}^{\mathrm{o}}\left[\{q_i^{(l)}(\mathbf{r})\}\right] \quad (16)$$

where

$$\Phi_{\mathrm{el}}^{\mathrm{o}}\left[\{q_i^{(l)}(\mathbf{r})\}\right]=\frac{\Gamma(\mathbf{r})^3}{3\pi}-\Gamma(\mathbf{r})l_{\mathrm{B}}\sum_i\left[\frac{z_i^2q_i^{(0)}(\mathbf{r})}{1+\Gamma(\mathbf{r})\sigma_i}+\frac{\gamma z_iq_i^{(1)}(\mathbf{r})}{1+\Gamma(\mathbf{r})\sigma_i}\right] \quad (17)$$

with $\gamma=\chi\sum_iq_i^{(2)}(\mathbf{r})z_i\{\Gamma(\mathbf{r})\sigma_i[1+\Gamma(\mathbf{r})\sigma_i]\}^{-1}$, where $\chi=\{3\sum_i q_i^{(3)}(\mathbf{r})[1+\Gamma(\mathbf{r})\sigma_i]^{-1}+[1-q^{(3)}(\mathbf{r})]\}^{-1}$ and $q^{(3)}(\mathbf{r})=\sum_iq_i^{(3)}(\mathbf{r})$. The first term in the right-hand side of Eq. (17) is the contribution from entropy, and the second term is the self-energy which is similar to the born energy. The space-dependent $\Gamma(\mathbf{r})$ can be defined in a similar way as the MSA for bulk electrolytes by requiring $\partial\Phi_{\mathrm{el}}[\{q_i^{(l)}(\mathbf{r})\}]/\partial\Gamma(\mathbf{r})=0$. Then we have

$$\Gamma^2=\pi l_{\mathrm{B}}\sum_i\frac{z_i^2q_i^{(0)}(\mathbf{r})}{(1+\Gamma\sigma_i)^2}+\pi l_{\mathrm{B}}\gamma\sum_i\frac{z_iq_i^{(1)}(\mathbf{r})}{(1+\Gamma\sigma_i)^2}+\pi l_{\mathrm{B}}\Gamma\frac{\partial\gamma}{\partial\Gamma}\sum_i\frac{z_iq_i^{(1)}(\mathbf{r})}{1+\Gamma\sigma_i} \quad (18)$$

where

$$\Gamma\frac{\partial\gamma}{\partial\Gamma}=3\gamma\chi\sum_i\frac{q_i^{(3)}(\mathbf{r})\Gamma\sigma_i}{(1+\Gamma\sigma_i)^2}-\chi\sum_i\frac{q_i^{(2)}(\mathbf{r})z_i(1+2\Gamma\sigma_i)}{\Gamma\sigma_i(1+\Gamma\sigma_i)^2} \quad (19)$$

In the bulk limit, Eq. (18) reduces to $\Gamma_{\mathrm{b}}^2=\pi l_{\mathrm{B}}\sum_i\rho_i^{\mathrm{b}}z_{\mathrm{eff},i}^2$ with ρ_i^{b} is the corresponding bulk density, where $z_{\mathrm{eff},i}=(z_i-0.5\gamma\Gamma\sigma_i^2)/(1+\Gamma\sigma_i)$ is the effective valency of species i and $l_{\mathrm{B}}=\beta e_0^2/(4\pi\varepsilon_0\varepsilon_{\mathrm{r}})$ is the Bjerrum length with e_0 the elementary charge and ε_0 and ε_{r} are the vacuum permittivity and relative dielectric constant of the background (which mimics the implicit solvent), respectively. Note that although we employ four FMT-like scalar weighted densities, our results are not substantially different from the ones from Roth and Gillespie's work in which only $\{q_0^{(i)}\}$ used.[50] These four FMT-like scalar weighted densities are chosen to be consistent with the weighted density terms in the MSA. Furthermore, since $\{q_i^{(1)}\}$ and $\{q_i^{(2)}\}$ can be obtained directly from $\{q_i^{(0)}\}$ one only need to calculate $\{q_i^{(0)}\}$ and $\{q_i^{(3)}\}$. Therefore, the time cost of calculating the four FMT-like scalar weighted densities is comparable to the calculation of $\{q_i^{(0)}\}$ only.

In Eq. (9), the chain connectivities due to the hard-core interactions $\mathcal{F}_{\mathrm{hs}}^{\mathrm{ch}}$ and the electrostatic correlations $\mathcal{F}_{\mathrm{el}}^{\mathrm{ch}}$ are, respectively,

$$\mathcal{F}_{\mathrm{hs}}^{\mathrm{ch}}[\{\rho_i(\mathbf{r})\}]=\sum_{i=p}^{P}\int\mathrm{d}\mathbf{r}\Phi_{\mathrm{hs},p}^{\mathrm{ch}}[\{n_l(\mathbf{r})\}] \quad (20)$$

and

$$\mathcal{F}_{\mathrm{el}}^{\mathrm{ch}}[\{\rho_i(\mathbf{r})\}]=\sum_{p=1}^{P}\int\mathrm{d}\mathbf{r}\Phi_{\mathrm{el},p}^{\mathrm{ch}}\left[\{q_i^{(l)}(\mathbf{r})\}\right] \quad (21)$$

The free energy density $\Phi_{\mathrm{hs},i}^{\mathrm{ch}}$ can be approximated by replacing the bulk densities in the first-order TPT treatment for uniform polymeric systems with the weighted densities as shown in Eq. (12), *i.e.*,[25]

$$\Phi_{\mathrm{hs},p}^{\mathrm{ch}}[\{n_l(\mathbf{r})\}]=\frac{n_0^p(\mathbf{r})}{\mathcal{N}_p}\left[\sum_{m=1}^{N_p}(1-N_p^m)\ln g_{m,m}^{\mathrm{hs},p}-\sum_{m=1}^{N_p-1}\ln g_{m,m+1}^{\mathrm{hs},p}\right] \quad (22)$$

with[51]

$$g_{m_1,m_2}^{\mathrm{hs},p}=\frac{1}{1-n_3}+\frac{n_2}{2(1-n_3)^2}\frac{\sigma_p^{m_1}\sigma_p^{m_2}}{\sigma_p^{m_1}+\sigma_p^{m_2}}+\frac{n_2^2}{18(1-n_3)^3}\left(\frac{\sigma_p^{m_1}\sigma_p^{m_2}}{\sigma_p^{m_1}+\sigma_p^{m_2}}\right)^2 \quad (23)$$

Analogously, the free energy density $\Phi_{\mathrm{el},p}^{\mathrm{ch}}$ can be approximated by

$$\Phi_{\mathrm{el},p}^{\mathrm{ch}}\left[\{q_i^{(l)}(\mathbf{r})\}\right]=\frac{q_p^{(0)}(\mathbf{r})}{\mathcal{N}_p}\times\left[\sum_{m=1}^{N_p}(1-N_p^m)y_{m,m}^{\mathrm{el},p}-\sum_{m=1}^{N_p-1}y_{m,m+1}^{\mathrm{el},p}\right] \quad (24)$$

with[21,22]

$$y_{m_1,m_2}^{\mathrm{el},p}=\frac{2l_{\mathrm{B}}\left[z_{m_1}z_{m_2}-z_{\mathrm{eff},m_1}z_{\mathrm{eff},m_2}\right]}{\sigma_p^{m_1}+\sigma_p^{m_2}} \quad (25)$$

In Eqs. (22) and (24), n_0^p and $q_p^{(0)}$ are the weighted densities for the total monomers of the p^{th} polymers.

The mean field Coulomb interaction $\mathcal{F}_{\mathrm{MF}}^{\mathrm{C}}$ has the form

$$\mathcal{F}_{\mathrm{MF}}^{\mathrm{C}}[\{\rho_i(\mathbf{r})\}]=\frac{1}{2}\sum_{i,j}\int\mathrm{d}\mathbf{r}_1\int\mathrm{d}\mathbf{r}_2\rho_i(\mathbf{r}_1)\rho_j(\mathbf{r}_2)\Psi_{ij}(\mathbf{r}_1,\mathbf{r}_2) \quad (26)$$

where $\Psi_{ij}(\mathbf{r}_1,\mathbf{r}_2)$ is the Coulomb interaction. In the point charge model, $\beta\Psi_{ij}(\mathbf{r}_1,\mathbf{r}_2)=\beta\Psi_{ij}^{\mathrm{C}}(\mathbf{r}_1,\mathbf{r}_2)=l_{\mathrm{B}}z_iz_j/|\mathbf{r}_1-\mathbf{r}_2|$, where z_i is the valency of ion species i. Eq. (26) can be rewritten as

$$\mathcal{F}_{\mathrm{MF}}^{\mathrm{C}}[\{\rho_i(\mathbf{r})\}]=\mathcal{F}_{\mathrm{MF}}^{\mathrm{sh}}[\{\rho_i(\mathbf{r})\}]+\sum_iz_ie_0\int\mathrm{d}\mathbf{r}\rho_i(\mathbf{r})\phi(\mathbf{r})-\int\mathrm{d}\mathbf{r}\frac{\varepsilon_0\varepsilon_{\mathrm{r}}}{2}[\nabla\phi(\mathbf{r})]^2 \quad (27)$$

where

$$\mathcal{F}_{\mathrm{MF}}^{\mathrm{sh}}[\{\rho_i(\mathbf{r})\}]=\frac{1}{2}\sum_{i,j}\int\mathrm{d}\mathbf{r}_1\int\mathrm{d}\mathbf{r}_2\rho_i(\mathbf{r}_1)\rho_j(\mathbf{r}_2)\Delta\Psi_{i,j}(\mathbf{r}_1,\mathbf{r}_2) \quad (28)$$

with $\Delta\Psi_{i,j}(\mathbf{r}_1,\mathbf{r}_2)=\Psi_{ij}(\mathbf{r}_1,\mathbf{r}_2)-\Psi_{ij}^{\mathrm{C}}(\mathbf{r}_1,\mathbf{r}_2)$. In Eq. (27), $\phi(\mathbf{r})$ is the electrostatic potential. It is known that the point charge model overcounts the electrostatic interaction in the mean-field treatment. Therefore, similar to the work in Ref. [50], we proposed a truncated charge shell model in our previous work,[49] where the charge was evenly distributed on the spherical shell with radius b_α. According to the truncated charge shell model, we have

$$\beta\Delta\Psi_{ij}(\mathbf{r}_1,\mathbf{r}_2)=\begin{cases}0 & \text{if } r_{12}\geq h_{ij}\\ -\dfrac{l_B z_i z_j}{4b_i b_j r_{12}}\left(r_{12}-b_{ij}\right)^2 & \text{if } |\Delta b_{ij}|\leq r_{12}<h_{ij}\\ l_B z_i z_j\left[\dfrac{1}{\max\{b_i,b_j\}}-\dfrac{1}{r_{12}}\right] & \text{if } 0<r_{12}<|\Delta b_{ij}|\end{cases} \tag{29}$$

with $b_{ij}=b_i+b_j$, $\Delta b_{ij}=b_i-b_j$, $h_{ij}=h_i+h_j$, and $r_{12}=|\mathbf{r}_1-\mathbf{r}_2|$, where b_i and h_i are the radius of the charge shell and the truncated length, respectively. In general, we have $\lambda_i=R_i+A/2\Gamma_b$ and $h_i=R_i+B/2\Gamma_b$. In this work, we set $A=1$ and $B=0$, *i.e.*, $b_i=\lambda_i$ and $h_i=R_i$. We have to note that although the radius of charge shell b_i is very large in dilute charge solutions, this truncated charge shell model is still reliable. In dilute charged solutions, the first term in the right-hand side of Eq. (27) is not important. The second and third terms will domain the mean field Coulomb interactions.

The free energy due to the van der Waals interactions $\mathcal{F}_{vdW}$ is usually treated using a mean-field approximation,[52] that is

$$\mathcal{F}_{vdW}[\{\rho_i(\mathbf{r})\}]=\frac{1}{2}\sum_{i,j}\int d\mathbf{r}_1\int d\mathbf{r}_2\rho_i(\mathbf{r}_1)\rho_j(\mathbf{r}_2)u_{ij}(\mathbf{r}_1,\mathbf{r}_2) \tag{30}$$

Usually, $u_{ij}(\mathbf{r}_1,\mathbf{r}_2)$ is modeled as Lennard-Jones potential, Yukawa potential, or Square-well potential. In *Atif*, we use Square-well potential, *i.e.*,

$$\beta u_{ij}(\mathbf{r}_1,\mathbf{r}_2)=\begin{cases}+\infty & r_{12}<\sigma_{ij}\\ \varepsilon_{ij} & \sigma_{ij}\leq r_{12}\leq\gamma_c\sigma_{ij}\\ 0 & r_{12}>\gamma_c\sigma_{ij}\end{cases} \tag{31}$$

where $\sigma_{ij}=(\sigma_i+\sigma_j)/2$ and the potential width parameter γ_c is fixed to 1.2 in *Atif* (which can be changed easily).

Combining Eqs. (4), (5) and (9), we obtain the full grand potential for the system considered in this work. Extremization of the grand potential Eq. (4) with respect to $\rho_p(\mathbf{R})$, $\rho_\alpha(\mathbf{r})$, $\phi(\mathbf{r})$ yields respectively the Euler-Lagrange equations for the density profiles of the polymers and small ions, and the Poisson equation:

$$\rho_p(\mathbf{R})a^{\mathcal{N}_p}=\exp\left\{\beta\left(\mu_p-V_p^b(\mathbf{R})-U_p^b(\mathbf{R})-\sum_{k=1}^{\mathcal{N}_p}\omega_p^k(\mathbf{r}_p^k)\right)\right\} \tag{32}$$

$$\rho_\alpha(\mathbf{r})a_\alpha=\exp\{\beta[\mu_\alpha-\omega_\alpha(\mathbf{r})]\} \tag{33}$$

$$\nabla^2\phi(\mathbf{r})=-\frac{e_0}{\varepsilon_r\varepsilon_0}\sum_i z_i\rho_i(\mathbf{r}) \tag{34}$$

In Eqs. (32) and (33), the effective fields $\{\omega_p^k(\mathbf{r})\}$ are

$$\omega_p^k(\mathbf{r})=\psi_{p,m}(\mathbf{r})+z_p^m e_0\phi(\mathbf{r})+\frac{\delta(\mathcal{F}_{hs}+\mathcal{F}_{vdW}+\mathcal{F}_{el}+\mathcal{F}_{MF}^{sh})}{\delta\rho_p^m(\mathbf{r})} \tag{35}$$

for $\sum_{\hat{m}=1}^{m-1}N_p^{\hat{m}}<k\leq\sum_{\hat{m}=1}^{m}N_p^{\hat{m}}$ with $\sum_{\hat{m}=1}^{0}N_p^{\hat{m}}=0$; and $\{\omega_\alpha(\mathbf{r})\}$ are

$$\omega_\alpha(\mathbf{r})=\psi_\alpha(\mathbf{r})+z_\alpha e_0\phi(\mathbf{r})+\frac{\delta(\mathcal{F}_{hs}+\mathcal{F}_{vdW}+\mathcal{F}_{el}+\mathcal{F}_{MF}^{sh})}{\delta\rho_\alpha(\mathbf{r})} \tag{36}$$

Substitution of Eq. (32) into Eq. (13), the density profile of the k^{th} segment in the p^{th} polymer can be obtained, that is,

$$\rho_p^k(\mathbf{r})a=\exp\left\{\beta\left[\mu_p-\omega_p^k(\mathbf{r})\right]\right\}\Omega_p^k(\mathbf{r}) \tag{37}$$

where

$$\Omega_p^k(\mathbf{r})=\begin{cases}\int e^{-\beta\omega_p^{k-1}(\mathbf{r}')}G_L^{k-1}(\mathbf{r}',\mathbf{r})d\mathbf{r}' & k=\mathcal{N}_p\\ \int e^{-\beta\omega_p^{k+1}(\mathbf{r}')}G_L^k(\mathbf{r},\mathbf{r}')G_R^k(\mathbf{r}',\mathbf{r})d\mathbf{r}' & k<\mathcal{N}_p\end{cases} \tag{38}$$

In Eq. (38), the propagators G_L^j and G_R^j are determined from the recurrence relations

$$G_L^k(\mathbf{r}_p^k,\mathbf{r}_p^{k+1})=\begin{cases}1 & k=1\\ \int\dfrac{\delta(|\mathbf{r}_p^k-\mathbf{r}'|-d_p^{k-1})}{4\pi d_p^{k-1}d_p^{k-1}}\exp\left[-\beta\omega_p^{k-1}(\mathbf{r}')\right]\times & \\ \varepsilon(\mathbf{r}',\mathbf{r}_p^k,\mathbf{r}_p^{k+1})G_L^{k-1}(\mathbf{r}',\mathbf{r}_p^k)d\mathbf{r}' & 1<k<\mathcal{N}_p\end{cases} \tag{39}$$

and

$$G_R^k(\mathbf{r}_p^{k+1},\mathbf{r}_p^k)=\begin{cases}\int\dfrac{\delta(|\mathbf{r}_p^{k+1}-\mathbf{r}'|-d_p^{k+1})}{4\pi d_p^{k+1}d_p^{k+1}}\exp\left[-\beta\omega_p^{k+2}(\mathbf{r}')\right]\times & \\ \varepsilon(\mathbf{r}_p^k,\mathbf{r}_p^{k+1},\mathbf{r}')G_R^{k+1}(\mathbf{r}_p^{k+1},\mathbf{r}')d\mathbf{r}' & k<\mathcal{N}_p-1\\ 1 & k=\mathcal{N}_p-1\end{cases} \tag{40}$$

where $\varepsilon(\mathbf{r}_p^k,\mathbf{r}_p^{k+1},\mathbf{r}_p^{k+2})=\exp\left[-\beta E_b(\mathbf{s}_p^k,\mathbf{s}_p^{k+1})\right]$.

Eqs. (33)–(38) can be solved numerically by Picard iteration constrained by specific boundary conditions. The numerical procedure starts with an initial guess for the density of each species $\{\rho_i(\mathbf{r})\}$ as input. Then the effective fields $\{\omega_p^k(\mathbf{r})\}$ and $\{\omega_p^\alpha(\mathbf{r})\}$ and propagators G_L^k and G_R^k are calculated, which result in the new density profiles $\{\rho_i^{new}(\mathbf{r})\}$. Then the new input densities are assigned by the following mixing rule: $\rho_i(\mathbf{r})=\rho_i(\mathbf{r})p_0+\rho_i^{new}(\mathbf{r})(1-p_0)$, where p_0 is a mixing parameter, typically on the order of 0.01. The procedure is repeated until the difference between successive iterations in the densities of $\{\rho_i^{new}(\mathbf{r})\}$ and $\{\rho_i(\mathbf{r})\}$ at all positions normalized by their respective bulk densities is less than an error tolerance e_{tot}, typically $e_{tot}=10^{-7}$. Some details about the numerical algorithm used in *Atif* are provided as follows. Firstly, the current *Atif* can only do one-dimensional calculations, *i.e.*, the density profiles of all species and electric potentials vary only in the direction perpendicular to the surface (z direction). Secondly, all the integrals are obtained numerically using Simpson integral method. Thirdly, the space-dependent screening parameter $\Gamma(\mathbf{r})$ are obtained using Newton-Raphson method based on Eq. (18). Finally, for one-dimensional calculations, the electric potential $\phi(z)$ is given by

$$\begin{aligned}\beta e_0\phi(z)=\beta e_0\phi(0)+4\pi l_B z\sum_i\int_0^\infty z_i\rho_i(z')dz'+\\ 4\pi l_B\sum_i\int_0^z z_i\rho_i(z')(z'-z)dz'\end{aligned} \tag{41}$$

The potential at the surface $\phi(0)$ is determined from the boundary conditions $d\phi(z)/dz|_{z=0}=-4\pi l_B Q$ (or $\phi(0)=\phi_0$) and $\phi(\infty)=0$, where Q is the surface charge density. We have to note that Eq. (41) is not robust for the systems with fixed surface charge density Q. In *Atif*, we use a smart method to obtain electric potential. We first obtain the pseudo electric potential $\phi^{pse}(z)$ based on the density profiles $\{\rho_i(z)\}$ *via*

$$\begin{aligned}\beta e_0\phi^{pse}(z)=4\pi l_B z\sum_i\int_z^\infty z_i\rho_i(z')dz'-\\ 4\pi l_B\sum_i\int_z^\infty z_i\rho_i(z')z'dz'\end{aligned} \tag{42}$$

Then we can get the new density profiles $\{\rho_i^*(z)\}$ based on the pseudo potential $\phi^{pse}(z)$. Usually, $\{\rho_i^*(z)\}$ does not satisfy

the charge neutrality condition. We introduce a parameter ϕ_0 that satisfies

$$e_0\sum_i\int_0^\infty z_i\rho_i^*(z')\exp(-\beta e_0 z_i\phi_0)\mathrm{d}z' = -Q \tag{43}$$

ϕ_0 can be obtained numerically. Then the electric potential is $\phi(z) = \phi^{\mathrm{pse}}(z) + \phi_0$ and the new density profiles are $\rho_i^{\mathrm{new}}(z) = \rho_i^*(z)\exp(-\beta e_0 z_i\phi_0)$.

Fig. 2 gives a schematic flowchart for the iterative numerical algorithm that is used to solve the Euler-Lagrange equations (Eqs. (33) and (37)) and Poisson equation (Eq. (34)) self-consistently. We have to note that Picard iteration algorithm is not the only option. Some other advanced numerical algorithms such as Newton-Raphson method and Broyden's method can be used to solve the self-consistent equations.[53] However, Picard iteration algorithm is very robust and efficient in one-dimensional calculations. A more advanced numerical method will be considered in three-dimensional calculations in *Atif* in the future. The framework of the main function of *Atif* is shown in Fig. 3.

Once a solution to Eqs. (33)–(38) is obtained, the grand potential of the whole system is calculated as

$$\beta W = \beta\mathcal{F}_{\mathrm{ex}} - \sum_\alpha\int \mathrm{d}\mathbf{r}\rho_\alpha(\mathbf{r})\left[\beta\hat{\omega}_\alpha(\mathbf{r}) + 1\right] - \sum_{p=1}^{P}\sum_{k=1}^{\mathcal{N}_i}\int \mathrm{d}\mathbf{r}\rho_p^k(\mathbf{r})\left[\beta\hat{\omega}_p^k(\mathbf{r}) + \frac{1}{\mathcal{N}_i}\right] \tag{44}$$

where $\hat{\omega}_\alpha = \omega_\alpha - \psi_\alpha$ and $\hat{\omega}_p^k = \omega_p^k - \psi_{p,m}$ with $\sum_{\hat{m}=1}^{m-1} N_p^{\hat{m}} < k \le \sum_{\hat{m}=1}^{m} N_p^{\hat{m}}$ and $\sum_{\hat{m}=1}^{0} N_p^{\hat{m}} = 0$.

INSTALLATION AND IMPLEMENTATION

The present contribution of this work is an attempt to remove the roadblock for researchers (especially experimental groups) to use self-consistent mean-field theory (SCFT) (see Sec. II in ESI) and DFT in studying the structural and thermodynamic properties of inhomogeneous complex fluids. There is no big obstacle for researchers with sufficient computational experience to compile the code. However, a significant barrier may exist to entry for potential users who do not do computational work. We thus provide the open-source *Atif* code including makefile as well as binary executables for OS X (named AtifOS) and Linux (named AtifLx) for public downloaded.[54] The computations through *Atif* is completely controlled by a readable input file. We are also providing the input files for all examples in this work. In this section, we will

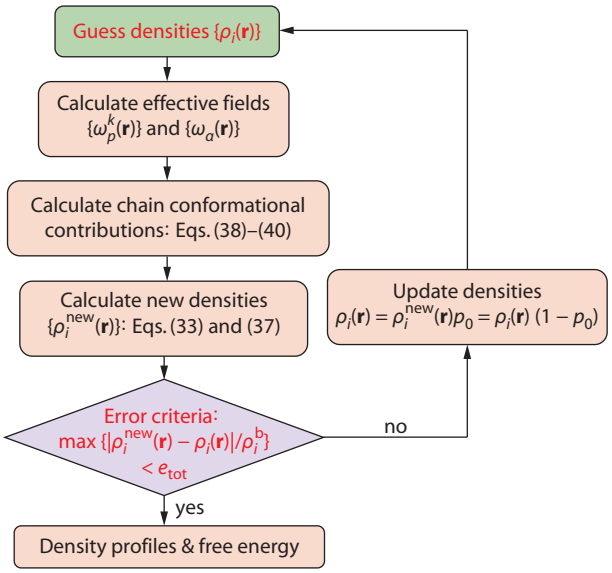

Fig. 2 A schematic flowchart for self-consistently solving the Euler-Lagrange equations and Poisson equation. In most cases, the bulk density of each species can be simply chosen as the initial guess density profiles, *i.e.*, $\rho_i(\mathbf{r}) = \rho_i^{\mathrm{b}}$. However, a better choice of the initial guess density profiles will accelerate the convergence.

```
int main( )
{
    readSystem();
    /*read all of the physical parameters from input file*/

    BulkChemPotential( );
    /*calculate the chemical potentials for each species*/

    FileOpen(); /*prepare the output files*/

    Initialization(); /*initialize the simulations*/

    do{

        EulerLagrange();
        /*solve the Euler-Lagrange equations as shown in
        Eqs. (32)–(40) with given density profiles {ρ_i(r)}*/

    }while(condition of convergence);

    EnergyCalculation(); /*Calculate the grand potential*/

    FileOutPut(); /*write the results in the output files*/

    return 0;
}
```

Prepare the simulation

Solve the Euler-Lagrange equations self-consistently as shown in Fig. 2

Output the results

Fig. 3 The pseudo-code for the main function of *Atif*.

```
=============================================================
/***********     The lines below are for the parameters of the system     ************/
=============================================================
1
|                                  ⋮
15
=============================================================
/********************     Set the path for the output files     ********************/
FILEPATH:
16 ~/Atif/output/examples/
=============================================================
```

Fig. 4 Part of the input file named "input_example.dat". The numbers as shown in the left-most column are the index of the lines, which do not actually exist in the input file.

briefly explain how to install and implement *Atif* on a Linux or OS X laptop.

To use *Atif*, we first need to download the source files, *i.e.*, "Atif.zip", from the website[54] and then uncompress them into our local path, *e.g.*, "~/". We can find the executables and makefile under the directory path "~/Atif/cmake/". One can use the existing executables or make a new executable file using the command "make". The example input files can be found under the directory path "~/Atif/example/". For the users who just want to know how to use *Atif* but not the theory or algorithm itself, they only need to understand the input file. We will explain the details of the input file in the next section via three illustrative examples, while in this section we will only demonstrate how to implement *Atif* without concerning the specific details in simulation. Before we run *Atif*, we have to assign the absolute directory path for the output files in the last line (see the 16th line in Fig. 4) in the input file. Then the following command (see Fig. 5) can be used to implement *Atif* in the background. Now, our first example is running in my laptop. In the next section, we will demonstrate the input file in detail *via* three specific examples.

```
echo "~/Atif/example/input_example.dat" | nohup ./AtifOS &
```

Fig. 5 In this example, the executable file named "AtifOS" is used. One can generate their own executable file using the command "make" under the directory path "~/Atif/cmake/".

CASE STUDIES

We demonstrate part of the applicability of *Atif via* three examples: 1, electric double-layer (EDL) of asymmetric electrolytes; 2, flexible/semi-flexible sequence-defined polyelectrolytes near a surface; 3, interactions between two surfaces mediated by polyelectrolyte solution. The operation of *Atif* is controlled by an input file that contains all the parameters of the mimic system. In this section, we will explain the input file in depth without concerning the details of the numerical procedures in *Atif*.

EDL of Asymmetric Electrolytes

The EDL of electrolytes has been studied extensively in the past and is still a hot topic in many fields such as supercapacitors. To predict correctly the EDL of electrolytes with asymmetrical ions is a particular challenge, especially for the cases when the external field is weak. However, in most cases, the cDFT can quantitatively predict the EDL compared to the Monte Carlo simulations based on the primitive model (which is a commonly used model for electrolyte systems in analytic theory, numerical computation, and molecular simulation). In this section, we demonstrate that our tool (*Atif*) can be used to accurately and easily study the electrolyte systems with size/valency asymmetry. In Fig. S1 in ESI, the parts of the input file specify all the physical parameters that determine an assigned electrolyte system with size/valency asymmetry is presented and the explanations of this input file are also provided. By using the similar command to the one shown in Fig. 5, one can obtain the EDL structure near a single surface. Fig. 6 shows the density profiles for cations (z_+ = 2, σ_+ = 6 Å, and 0.1 M) and anions (z_=1, σ_- = 3 Å and 0.2 M) in the vicinity of a neutral surface. In order to show the advance of *Atif*, we will provide comparisons between *Atif* and other theoretical methods such as a DFT method based on the bulk fluid density (BFD) expansion proposed by Wu's group,[1] a DFT method based on the reference fluid density (RFD) expansion proposed by Gillespie and coworkers,[55] and the self-consistent mean-field theory (SCFT, see Sec. II in ESI). Both in BFD and RFD methods, the mean field Coulomb interactions are calculated based on a point charge model (*i.e.*, $\mathcal{F}_{MF}^{sh}$ = 0) and the electrostatic correlations are obtained using Taylor expansion. In *Atif*, the mean field Coulomb interactions are calculated using a truncated charge shell model (Eq. 29) and the electrostatic correlations are obtained using a FMT-like weighted density approximation (Eqs. 15–19). According to Fig. 6, we know that both BFD (orange curves) and SCFT (blue curves) cannot provide even qualitative predictions for both cations and anions in such a strongly asymmetrical system. However, the predictions (red curves) from *Atif* (red curves) and RFD (cyan curves) show excellent agreement with the ones from MC simulations (black circles). More specifically, *Atif* shows much better predictions than RFD close to the surface; while RFD shows better predictions than *Atif* in the area far from the surface. One can refer to our previous work[49] to see more direct comparisons between cDFT calculations and MC simulations for inhomogeneous electrolyte systems. In Fig. 6, we also provide the simulation time consumption of each method under the same simulation conditions, *i.e.*, the same simulation parameters and Central Processing Unit (Intel Xeon Platinum 9242 CPU 2.30GHz). The time consumption of *Atif*, BFD, RFD, and SCFT are 0.63, 24.73, 40.32, and 0.05 minutes, respectively. In a word, both in terms of the accuracy and the efficiency, *Atif* is an advanced theoretical tool.

Flexible/Semi-flexible Sequence-defined Polyelectrolytes Near a Surface

Polyelectrolyte (PE) is a polymer whose repeating units can be

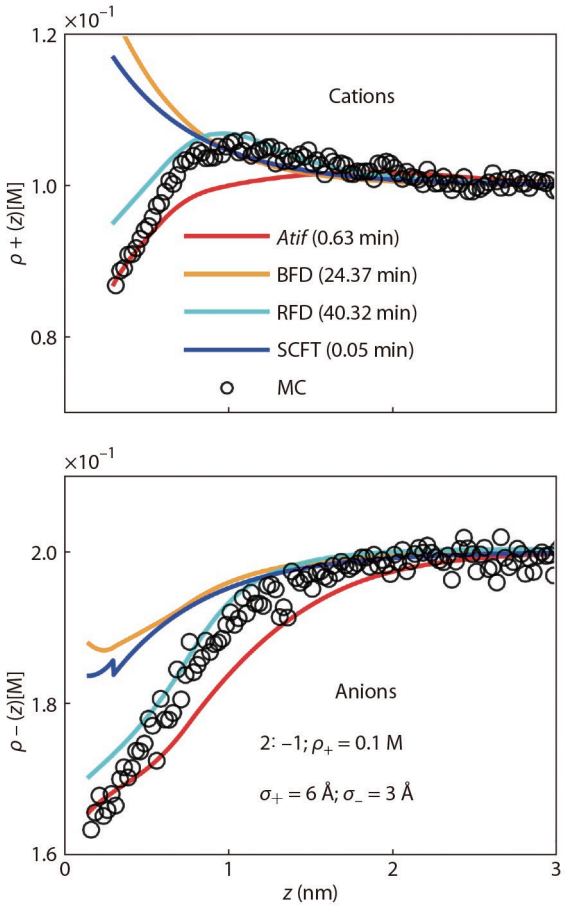

Fig. 6 The density profiles for cations (top) and anions (bottom) for 2:−1 electrolytes near a neutral surface. The diameters are σ_+ = 6 Å and σ_- = 3 Å and the ion concentration is 0.1 M. The temperature and dielectric constant are 298.15 K and 78.5, respectively, to mimic room temperature aqueous solution. The numbers in the parentheses in the top figure are the time consumptions of each methods with unit minutes (mins). "MC" (black circle) means GCMC.[56] The corres ponding input file is shown in Fig. S1 in Sec. III of ESI.

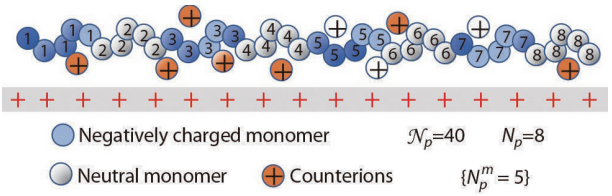

Fig. 7 Schematic of the sequence-defined semiflexible polyelectrolytes (AB-type multiblock copolymers). The blue and light gray blocks are the negatively charged and neutral monomers, respectively. The dark orange spheres denote the positive counterions and the gray filling rectangle is the charged surface. $\mathcal{N}_p$ and N_p are the degree of polymerization and number of blocks, respectively. N_p^m is the number of monomers of block m.

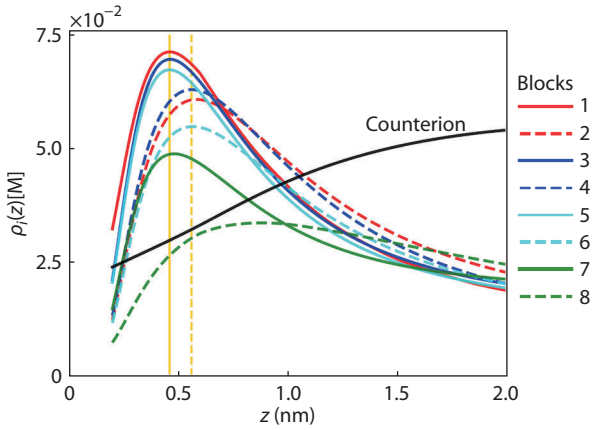

Fig. 8 The density profiles for monomers and counterions near a charged surface. The diameters for monomers and counterions are σ = 4 Å and the monomer concentration is 0.1 M. The surface charge density and bending potential are 0.02 C/m^2 and κ_b = 10. The temperature and dielectric constant are 298.15 K and 78.5, respectively. The solid and dash vertical lines show the peak positions of the charged blocks and non-terminal neutral blocks, respectively. The corresponding input file is shown in Fig. S2 in ESI.

partially or fully charged in a specific solvent. The sequence of monomers along a polyelectrolyte chain can have a significant impact on the surface and interfacial properties and structure and function of its self-assembly materials.[57–59] In this section, we will not discuss the effects of monomer sequence on the surface/interfacial or self-assembly properties. We will only explain how to use *Atif* to study structure and thermodynamic properties of sequence-defined polyelectrolytes (PEs) near a single surface (see Fig. 7). The parts of the input file that contain the physical parameters for a given sequence-defined polyelectrolyte systems are provided in Fig. S2 in ESI and the corresponding explanations are also presented. In Fig. 8, the density profiles for AB (alternating) multiblock copolymers are shown, where block A is fully charged and block B is neutral. The total number of blocks is N_p = 8 and each block consists of 5 monomers, *i.e.*, $N_p^1 = N_p^2 = \cdots = N_p^8 = 5$. That is, the degree of polymerization is $\mathcal{N}_p$ = 40 (see Fig. 7). According to Fig. 8, we know that the charged blocks prefer to accumulate at the surface due to the electrostatic attraction. Although the peaks of the density distributions for different charged blocks are almost at the same position, the magnitude of the peaks are quite different. The peak magnitude of the 7th block (the green solid curve in Fig. 8) is much smaller than the ones of the other charged blocks due to the suspending end block (the green dash curve in Fig. 8). The non-terminal neutral (athermal) blocks also show remarkable accumulation near the surface, where the peak positions of the density profiles of the non-terminal neutral blocks are farther than the ones of the charged blocks. Those phenomena mentioned above are predictable. In fact, the surface and interfacial behaviors of sequence-defined PEs are rich and complicated.[33] The systematical study on this issue will be discussed in our future work. It is worth noting that in this work we only take a simple AB alternating semiflexible copolymer as example. Actually, *Atif* can be used to investigate surface and interfacial properties for arbitrary linear flexible/semiflexible polymers or polymer blends systems based on the tangentially connected hard-sphere model.

Interactions Between Two Surfaces Mediated by Polyelectrolyte Solution

Polymers play an important role in industrial manufacture. For

example, PEs are extensively used as additives in broad applications, such as flocculation and stabilization of colloidal suspensions, emulsions and foams, water purification, papermaking and so on.[60–62] For this reason, the studies of the interaction between surfaces mediated by PE solutions attract a lot of attention of researchers. In this section, we will demonstrate how to calculate PE solution-induced interactions between two charged surfaces (the schematic of this system is shown in Fig. 9). For a given separation distance h between two charged surfaces, we can calculate the grand potential $W(h)$ using Eq. (44). Then the osmotic pressure is $\Pi(h) = -\partial w(h)/\partial h$ where $w = W/A$ with A the area of each surface and the force per unit area between the two surfaces with separation distance h is $\Pi(h) - \Pi(\infty)$. In this work, the osmotic pressure for the confined system with separation distance h is estimated by

$$\Pi(h) \approx \frac{w(h) - w(h + 0.01\sigma)}{0.01\sigma} \quad (45)$$

According to Eq. (45), we can obtain the h-dependent osmotic pressure $\Pi(h)$. According to Fig. 10, the interactions between the two charged surfaces under the conditions considered in this section are pure repulsion when $h > \sigma$ due to the EDL overlapping, and the two surfaces will not feel each other when $h > 6\sigma$. Although the behavior of PE solution-induced interactions shown here seems simple and obvious, it can be very interesting and complicated in other parameter space.[63,64] One can use *Atif* to explore broad parameter space for better understanding the interaction behaviors of confined systems with different kinds of polymers or/and salts. In this work, we only show one simple example to explain how to calculate the interactions between two surface using *Atif*.

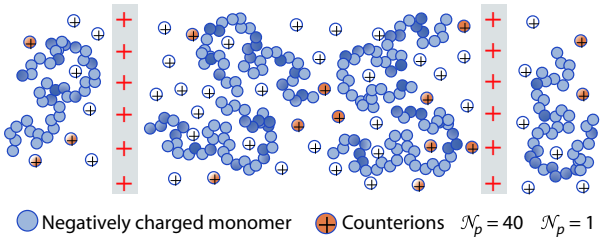

Fig. 9 Schematic of the model for PE solution confined in two charged surfaces. The blue and light gray and isolated dark orange spheres are the negatively charged monomers and positive counterions, respectively. The gray filling rectangles are the two charged surfaces. $\mathcal{N}_p$ and N_p are the degree of polymerization and the number of blocks, respectively.

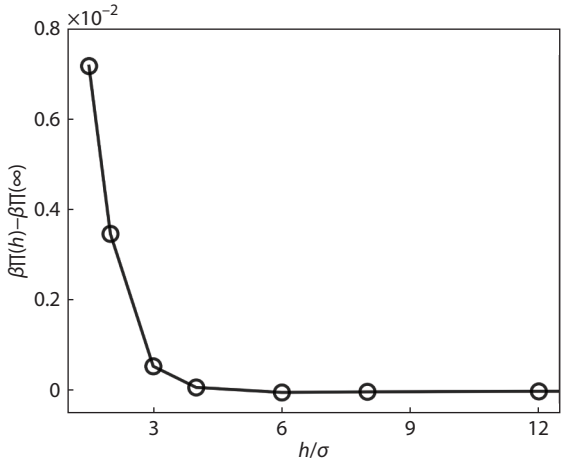

Fig. 10 PE solution-induced interactions between two charged surfaces. The bending potential and the monomer concentration are $\kappa_b = 0$ and 0.1 M, respectively. The other parameters are the same as the ones in Fig. 8. The corresponding input file is shown in Fig. S3 in ESI.

CONCLUSIONS

Classical density functional theory (cDFT), as an advanced theoretical method, has proven to be a sophisticated, robust, and efficient approach for studying the structural and thermodynamic properties of inhomogeneous complex fluids. However, cDFT is more esoteric compared to other theoretical and simulation methods, such as self-consistent field theory (SCFT) and Monte Carlo simulation and so on. Therefore, there are big roadblocks in the extensive use of cDFT. In this work, our goal is to build a bridge between cDFT and the researchers who are interested in complex fluid systems.

We have presented three examples to pedagogically introduce an easy-to-use and broadly accessible open-source cDFT software package named "an advanced theoretical tool for inhomogeneous fluids" (*Atif*). Although, in this work, we only consider simple systems such as asymmetric salts or simple semiflexible block copolymers in the vicinity of a single charged surface and flexible polyelectrolytes confined by two charged surfaces, *Atif* can be used to study various systems with symmetric/asymmetric salts or/and almost all kinds of linear flexible/semiflexible polymers (including polymer blends). And the interactions between species and surfaces are optional, *i.e.*, electrostatic, non-electrostatic, or both. Moreover, *Atif* can be used to study systems with dielectric constant discontinuity across the surface-solution interface. Additionally, one can easily extend *Atif* to investigate other systems which have not yet been covered by our original version of *Atif* such as polymer brush systems. Therefore, it is expectable that one can use *Atif* to explore new and interesting physical phenomena in inhomogeneous complex fluid systems. It is worth noting that the current *Atif* can only be used to consider systems with planar surfaces and do one dimensional calculations. Our group will keep update on the new version of *Atif*. In the near future, we will add modules to involve spherical and cylindrical surfaces. And consideration of two and three dimensional systems in *Atif* are also in our plan.

NOTES

The author declares no competing financial interest.

Electronic Supplementary Information

Electronic supplementary information (ESI) is available free of charge in the online version of this article at http://doi.org/10.1007/s10118-021-2646-4.

ACKNOWLEDGMENTS

This work was financially supported by the National Natural Science Foundation of China (No. 21973104). This work was carried out at the National Supercomputer Center in Tianjin, and the calculations were performed on TianHe-1 (A).

REFERENCES

1 Yu, Y. X.; Wu, J.; Gao, G. H. Density-functional theory of spherical electric double layers and Zeta potentials of colloidal particles in restricted-primitive-model electrolyte solutions. *J. Chem. Phys.* **2004**, *120*, 7223–7233.
2 Wu, J. Density functional theory for chemical engineering: from capillarity to soft materials. *AIChE J.* **2006**, *52*, 1169–1193.
3 Wu, J.; Li, Z. Density-functional theory for complex fluids. *Annu. Rev. Phys. Chem.* **2007**, *58*, 85–112.
4 Hohenberg, P.; Kohn, W. Inhomogeneous electron gas. *Phys. Rev.* **1964**, *136*, B864–B871.
5 Mermin, N. D. Thermal properties of the inhomogeneous electron gas. *Phys. Rev.* **1965**, *137*, A1441–A1443.
6 Evans, R. The nature of the liquid-vapour interface and other topics in the statistical mechanics of non-uniform, classical fluids. *Adv. Phys.* **1979**, *28*, 143–200.
7 Tarazona, P. A density functional theory of melting. *Mol. Phys.* **1984**, *52*, 81–96.
8 Rosenfeld, Y. Free-energy model for the inhomogeneous hard-sphere fluid mixture and density-functional theory of freezing. *Phys. Rev. Lett.* **1989**, *63*, 980–983.
9 Mier-y-Teran, L.; Suh, S. H.; White, H. S.; Davis, H. T. A nonlocal free-energy density-functional approximation for the electrical double layer. *J. Chem. Phys.* **1990**, *92*, 5087–5098.
10 Tang, Z.; Scriven, L. E.; Davis, H. T. A three-component model of the electrical double layer. *J. Chem. Phys.* **1992**, *97*, 494–503.
11 Kierlik, E.; Rosinberg, M. L. Free-energy density functional for the inhomogeneous hard-sphere fluid: application to interfacial adsorption. *Phys. Rev. A* **1990**, *42*, 3382–3387.
12 Woodward, C. E.; Yethiraj, A. Density functional theory for inhomogeneous polymer solutions. *J. Chem. Phys.* **1994**, *100*, 3181–3186.
13 Li, Z.; Wu, J. Density functional theory for polyelectrolytes near oppositely charged surfaces. *Phys. Rev. Lett.* **2006**, *96*, 048302–048305.
14 Wertheim, M. S. Fluids with highly directional attractive forces. I. Statistical thermodynamics. *J. Stat. Phys.* **1984**, *35*, 19–34.
15 Wertheim, M. S. Fluids with highly directional attractive forces. II. Thermodynamic perturbation theory and integral equations. *J. Stat. Phys.* **1984**, *35*, 35–47.
16 Wertheim, M. S. Fluids with highly directional attractive forces. III. Multiple attraction sites. *J. Stat. Phys.* **1986**, *42*, 459–476.
17 Wertheim, M. S. Fluids with highly directional attractive forces. IV. Equilibrium polymerization. *J. Stat. Phys.* **1986**, *42*, 477–492.
18 Wertheim, M. S. Fluids of dimerizing hard spheres, and fluid mixtures of hard spheres and dispheres. *J. Chem. Phys.* **1986**, *85*, 2929–2936.
19 Wertheim, M. S. Thermodynamic perturbation theory of polymerization. *J. Chem. Phys.* **1987**, *87*, 7323–7331.
20 Wertheim, M. S. Integral equation for the Smith-Nezbeda model of associated fluids. *J. Chem. Phys.* **1988**, *88*, 1145–1155.
21 Jiang, J. W.; Liu, H.; Hu, Y.; Prausnitz, J. M. A molecular-thermodynamic model for polyelectrolyte solutions. *J. Chem. Phys.* **1998**, *108*, 780–784.
22 Jiang, J. W.; Blum, L.; Bernard, O.; Prausnitz, J. M. Thermodynamic properties and phase equilibria of charged hard sphere chain model for polyelectrolyte solutions. *Mol. Phys.* **2001**, *99*, 1121–1128.
23 Yu, Y. X.; Wu, J. Structures of hard-sphere fluids from a modified fundamental-measure theory. *J. Chem. Phys.* **2002**, *117*, 10156–10164.
24 Roth, R.; Evans, R.; Lang, A.; Kahl, G. Fundamental measure theory for hard-sphere mixtures revisited: the White Bear version. *J. Phys.: Condens. Matter* **2002**, *14*, 12063–12078.
25 Jiang, J.; Ginzburg, V. V.; Wang, Z. G. Density functional theory for charged fluids. *Soft Matter* **2018**, *14*, 5878–5887.
26 Blum, L. Mean spherical model for asymmetric electrolytes. *Mol. Phys.* **1975**, *30*, 1529–1535.
27 Blum, L.; Hoeye, J. S. Mean spherical model for asymmetric electrolytes. 2. Thermodynamic properties and the pair correlation function. *J. Phys. Chem.* **1977**, *81*, 1311–1316.
28 Hiroike, K. Supplement to Blum's theory for asymmetric electrolytes. *Mol. Phys.* **1977**, *33*, 1195–1198.
29 Forsman, J.; Nordholm, S. Polyelectrolyte mediated interactions in colloidal dispersions: hierarchical screening, simulations, and a new classical density functional theory. *Langmuir* **2012**, *28*, 4069–4079.
30 Forsman, J. Polyelectrolyte adsorption: electrostatic mechanisms and nonmonotonic responses to salt addition. *Langmuir* **2012**, *28*, 5138–5150.
31 Sandia National Laboratories, Tramonto. https://software.sandia.gov/tramonto/index.html.
32 Jiang, J. Non-monotonic effects of intrinsic stiffness and concentration of polyelectrolytes on the electro-sorption. *Macromolecules* **2021**, *54*, 1801–1810.
33 Chang, Q.; Jiang, J. Adsorption of block-polyelectrolytes on an oppositely charged surface. *Macromolecules* **2021**, *54*, 4145–4153.
34 Kratky, O.; Porod, G. Röntgenuntersuchung gelöster Fadenmoleküle. *Recl. Trav. Chim. Pays-Bas* **1949**, *68*, 1106–1122.
35 Grosberg, A. Y.; Khokhlov, A. R.; Onuchic, J. N. Statistical physics of macromolecules. *Phys. Today* **1995**, *48*, 92–93.
36 Rubinstein, M.; Colby, R. In *Polymer Physics*; Rubinstein, M., Colby, R., Eds.; Oxford University Press: New York: NY, USA, **2003**.
37 Reisner, W.; Pedersen, J. N.; Austin, R. H. DNA confinement in nanochannels: physics and biological applications. *Rep. Prog. Phys.* **2012**, *75*, 106601–106634.
38 Köster, S.; Weitz, D. A.; Goldman, R. D.; Aebi, U.; Herrmann, H. Intermediate filament mechanics in vitro and in the cell: from coiled coils to filaments, fibers and networks. *Curr. Opin. Cell Biol.* **2015**, *32*, 82–91.
39 Marantan, A.; Mahadevan, L. Mechanics and statistics of the worm-like chain. *Am. J. Phys.* **2018**, *86*, 86.
40 Honnell, K. G.; Curro, J. G.; Schweizer, K. S. Local structure of semiflexible polymer melts. *Macromolecules* **1990**, *23*, 3496–3505.
41 Phan, S.; Kierlik, E.; Rosinberg, M. L.; Yethiraj, A.; Dickman, R. Perturbation density functional theory and Monte Carlo simulations for the structure of hard triatomic fluids in slitlike pores. *J. Chem. Phys.* **1995**, *102*, 2141–2150.
42 Forsman, J.; Woodward, C. E. An improved density functional description of hard sphere polymer fluids at low density. *J. Chem. Phys.* **2003**, *119*, 1889–1892.
43 Cao, D.; Wu, J. Density functional theory for semiflexible and cyclic polyatomic fluids. *J. Chem. Phys.* **2004**, *121*, 4210–4220.
44 Forsman, J.; Woodward, C. E. Surface forces in solutions

containing rigid polymers: approaching the rod limit. *Macromolecules* **2006**, *39*, 1269–1278.
45 Turesson, M.; Forsman, J.; Åkesson, T. Surface forces mediated by charged polymers: effects of intrinsic chain stiffness. *Langmuir* **2006**, *22*, 5734–5741.
46 Turesson, M.; Woodward, C. E.; Åkesson, T.; Forsman, J. simulations of surface forces in polyelectrolyte solutions. *J. Phys. Chem. B* **2008**, *112*, 5116–5125.
47 Egorov, S. A.; Milchev, A.; Virnau, P.; Binder, K. Semiflexible polymers under good solvent conditions interacting with repulsive walls. *J. Chem. Phys.* **2016**, *144*, 174902–174914.
48 Milchev, A.; Binder, K. How does stiffness of polymer chains affect their adsorption transition? *J. Chem. Phys.* **2020**, *152*, 064901.
49 Jiang, J.; Gillespie, D. Revisiting the charged shell model: a density functional theory for electrolytes. *Journal of Chemical Theory and Computation* **2021**, *17*, 2409–2416.
50 Roth, R.; Gillespie, D. Shells of charge: a density functional theory for charged hard spheres. *J. Phys.: Condens. Matter* **2016**, *28*, 244006–244015.
51 Jiang, J.; Xu, X.; Huang, J.; Cao, D. Density functional theory for rod-coil polymers with different size segments. *J. Chem. Phys.* **2011**, *135*, 054903–054911.
52 Patra, C. N.; Yethiraj, A. Generalized van der Waals density functional theory for nonuniform polymers. *J. Chem. Phys.* **2000**, *112*, 1579–1584.
53 Eyert, V. A comparative study on methods for convergence acceleration of iterative vector sequences. *J. Comput. Phys.* **1996**, *124*, 271–285.
54 Jiang, J. Atif (an Advanced Theoretical Tool for Inhomogeneous Fluids). https://github.com/jiangj-physchem/Atif.
55 Gillespie, D.; Nonner, W.; Eisenberg, R. S. Coupling Poisson-Nernst-Planck and density functional theory to calculate ion flux. *J. Phys.: Condens. Matter* **2002**, *14*, 12129–12145.
56 Valiskó, M.; Kristóf, T.; Gillespie, D.; Boda, D. A systematic Monte Carlo simulation study of the primitive model planar electrical double layer over an extended range of concentrations, electrode charges, cation diameters and valences. *AIP Adv.* **2018**, *8*, 025320–025329.
57 Bates, F. S.; Hillmyer, M. A.; Lodge, T. P.; Bates, C. M.; Delaney, K. T.; Fredrickson, G. H. Multiblock polymers: Panacea or Pandora's box? *Science* **2012**, *336*, 434–440.
58 Lutz, J.F.; Ouchi, M.; Liu, D. R.; Sawamoto, M. Sequence-controlled polymers. *Science* **2013**, *341*, 1238149.
59 Lutz, J.F.; Lehn, J.M.; Meijer, E. W.; Matyjaszewski, K. From precision polymers to complex materials and systems. *Nat. Rev. Mater.* **2016**, *1*, 16024–16037.
60 Bolto, B.; Gregory, J. Organic polyelectrolytes in water treatment. *Water Res.* **2007**, *41*, 2301–2324.
61 Howe, A. M.; Wesley, R. D.; Bertrand, M.; Côte, M.; Leroy, J. Controlled association in suspensions of charged nanoparticles with a weak polyelectrolyte. *Langmuir* **2006**, *22*, 4518–4525.
62 Claesson, P. M.; Dedinaite, A.; Rojas, O. J. Polyelectrolytes as adhesion modifiers. *Adv. Colloid Interface Sci.* **2003**, *104*, 53–74.
63 Jiang, J.; Ginzburg, V. V.; Wang, Z. G. On the origin of oscillatory interactions between surfaces mediated by polyelectrolyte solution. *J. Chem. Phys.* **2019**, *151*, 214901.
64 Balzer, C.; Jiang, J.; Marson, R. L.; Ginzburg, V. V.; Wang, Z. G. Nonelectrostatic adsorption of polyelectrolytes and mediated interactions between solid surfaces. *Langmuir* **2021**, *37*, 5483–5493.

https://doi.org/10.1007/s10118-021-2646-4